HHS Public Access
Author manuscript
Gene Expr Patterns. Author manuscript; available in PMC 2019 September 01.

Published in final edited form as:
Gene Expr Patterns. 2018 September ; 29: 82–87. doi:10.1016/j.gep.2018.07.002.

Developmental expression of the zebrafish Arf-like small GTPase paralogs *arl13a* and *arl13b*

Ping Song and **Brian D. Perkins**
Department of Ophthalmic Research, Cole Eye Institute, Cleveland Clinic, Cleveland, OH 44195

Abstract

Members of the Arf-like (Arl) family of small GTP-binding proteins regulate a number of cellular functions and play important roles in cilia structure and signaling. The small GTPase Arl13a is a close paralog to Arl13b, a small GTPase required for normal cilia formation that causes Joubert Syndrome when mutated. As mutation of *arl13b* causes a slow retinal degeneration in zebrafish (Song et al., 2016), we hypothesized that expression of *arl13a* may provide functional redundancy. We determined the expression domains of *arl13a* and *arl13b* during zebrafish development and examined subcellular localization by expression of fluorescence fusion proteins. Both genes are widely expressed during early cell division and gastrulation and Arl13a and Arl13b both localize to microtubules in ciliated and dividing cells of the early zebrafish embryo. Between 2–5 days post fertilization (dpf), *arl13b* is expressed in neural tissues while expression of *arl13a* is downregulated by 2 dpf and restricted to craniofacial structures. These results indicate that *arl13a* and *arl13b* have evolved different roles and that *arl13a* does not function in the zebrafish retina.

Keywords

photoreceptor; cilia; Joubert Syndrome; zebrafish

Introduction

Cilia are microtubule-based organelles that protrude from the surface of most eukaryotic cells (Satir and Christensen, 2007) and can be classified as motile cilia or non-motile (primary) cilia. Motile cilia function to drive locomotion in single-celled eukaryotes and gametes, or to propel fluid across the cell surface (Roy, 2009). Primary cilia function as sensory organelles and monitor the extracellular environment by concentrating receptors within the ciliary membrane (Malicki and Johnson, 2016). It is now well established that cilia are necessary for detecting a diverse range of signals, including light, hormones, neurotransmitters, morphogens, and growth factors (Ishikawa and Marshall, 2011; Hilgendorf et al., 2016). Given the importance of ciliary function for normal development

Correspondence To: Brian D. Perkins, Ph.D., Cole Eye Institute, Cleveland Clinic, 9500 Euclid Ave. Cleveland, OH 44195, (216) 444-9683, perkinb2@ccf.org.

and physiology, it is not surprising that defects in cilia can result in a number of pleiotropic genetic diseases, termed ciliopathies (Sharma et al., 2008). Joubert Syndrome (JBTS), Leber Congenital Amaurosis (LCA), Meckel Syndrome (MKS) Bardet-Biedl Syndrome (BBS), and Nephronophthisis (NPHP) are ciliopathies with overlapping clinical features, including retinal degeneration, obesity, polydactyly, skeletal abnormalities, and defects in hepatic, respiratory, and renal function (Sharma et al., 2008).

Three members of the ADP-ribosylation-factor-like (Arl) family of small G-proteins (Arl6, Arl3, and Arl13b) play important roles in cilia biogenesis (Li et al., 2010; Li et al., 2012). Arl6 was the first member of the Arl family shown to cause disease when it was identified in a set of genes found to cause BBS (Chiang et al., 2004; Fan et al., 2004). Also known as Bbs3, Arl6 localized to the basal body in a ring-shaped pattern in hTERT cells (Wiens et al., 2010). Although not detected within the cilium of wild-type cells, it is thought that Arl6 facilitates ciliary exit of the BBSome, the large complex of BBS proteins required for ciliary membrane biogenesis (Nachury et al., 2007; Liew et al., 2014). A role for Arl3 in cilia function was first identified in the protozoan *Leishmania donovani* (Cuvillier et al., 2000). Subsequent work found that Arl3 directly binds with RP2 (retinitis pigmentosa protein 2), which functions as the GAP (GTPase activating protein) for Arl3 (Veltel et al., 2008). Both RP2 and Arl3 localize to the connecting cilium of photoreceptors (Grayson et al., 2002). Arl3 has been linked to the trafficking of lipidated membrane-associated proteins (Hanke-Gogokhia et al., 2016a; Hanke-Gogokhia et al., 2016b). Defects Arl3-mediated trafficking of prenylated proteins in rod photoreceptors led to cell death and retinal degeneration (Wright et al., 2016) Although human mutations in *ARL3* have not yet been identified, the *Arl3*$^{-/-}$ knockout mice exhibit phenotypes consistent with ciliary defects (Schrick et al., 2006). Unlike Arl6 and Arl3, which function both inside and outside the cilium, localization of Arl13b is limited to primary cilia. Arl13b was first linked to cilia in a forward genetic screen for kidney cysts in zebrafish (Sun et al., 2004). Shortly thereafter, the mouse *Arl13b*^{hnn} mutant was described as having defects in neural tube patterning, shortened cilia, and polydactyly, which were phenotypes consistent with cilia defects (Caspary et al., 2007). Mutations in *ARL13B* were subsequently identified in families with Joubert Syndrome (Cantagrel et al., 2008). Arl13b has been proposed to function at the guanine nucleotide exchange factor (GEF) for Arl3, thereby spatially restricting Arl3 activation and cargo release to the cilium (Gotthardt et al., 2015).

Mutations disrupting the structure or function of cilia in zebrafish lead to a common set of phenotypes that include rapid photoreceptor cell death, kidney cysts, left-right asymmetry, and a curly body axis (Sun et al., 2004; Tsujikawa and Malicki, 2004; Pathak et al., 2007; Omori et al., 2008). Zebrafish lacking *arl13b* exhibit many of these phenotypes (Sun et al., 2004). We recently reported, however, that zebrafish *arl13b*$^{-/-}$ mutants undergo a slow, progressive photoreceptor degeneration (Song et al., 2016). While the *arl13b*$^{-/-}$ mutants develop kidney cysts during larval stages and exhibit phenotypes seen in other zebrafish cilia mutants, the mild retinal phenotype was unusual. One possible explanation for these results is functional redundancy with a closely related protein. Here, we explored the hypothesis that Arl13a may compensate for Arl13b in zebrafish photoreceptor function. Cellular localization studies revealed that Arl13a colocalized to microtubules in both ciliated and dividing cells of early zebrafish embryos. We report, however, that while *arl13a* expression overlaps with *arl13b* during early zebrafish development, the expression patterns differed at later stages during neural differentiation. We conclude that Arl13a likely does not compensate for Arl13b in the zebrafish retina.

METHODS

Zebrafish care and maintenance

Zebrafish were maintained in a 14:10 hr light-dark cycle on Aquatic Habitats recirculating water systems (Pentair; Apopka, FL). Animals were maintained in accordance with protocols approved by the Cleveland Clinic Institutional Animal Care and Use Committee (IACUC). To image and localize basal bodies, we used the transgenic line *Tg(5actb2:cetn2-GFP)* ^{cu6}, which expresses a centrin2-GFP fusion protein from the β-actin promoter (Randlett et al., 2011). The *arl13b (sco)*^{hi459} line was previously described (Sun et al., 2004; Song et al., 2016).

In situ hybridization and immunocytochemistry

Localization of mRNA by *in situ* hybridization was done using digoxigenin-and fluorescein-labeled riboprobes as described (Jowett, 2001). The full -length zebrafish *arl13a* cDNA clone (NCBI Reference Sequence: NM_200818.1) was purchased from ATCC (ID 10167628). The full-length zebrafish *hmx4* cDNA clone was purchased from GE Dharmacon via Thermo Scientific. The *pax2a* clone was previously described (Perkins et al., 2005). Images were obtained on a Zeiss AxioZoom.V16 fluorescence stereomicroscope using an AxioCam digital camera (Carl Zeiss Microscopy, Thornberg, NY).

Whole-mount immunostaining was performed as described previously (Lunt et al., 2009). A monoclonal antibody against acetylated α-tubulin (Clone 6–11B-1, Sigma, St Louis, MO) was used at 1:100 dilution to identify cilia. Centrosomes were labeled with a monoclonal anti-γ-tubulin antibody (Sigma, GTU-88) at 1:5000 dilution. Spindle microtubules were labeled with a monoclonal antibody against anti-alpha-tubulin (Clone T9026, Sigma) used at 1:500 dilution. Rabbit polyclonal antibodies against mCherry (Catalog number 5993; BioVision, Milpitas, CA) were used at 1:400 dilution to detect the Arl13a-mCherry fusion protein. Chicken polyclonal antibodies against GFP (Catalog number 13970; Abcam; Cambridge, MA) were used at 1:500 dilution to detect GFP. Alexa secondary antibodies (Invitrogen) were diluted 1:500 and used for fluorescent detection. Embryos for whole-mount immunohistochemistry were mounted on depression slides in PBST. Serial optical sections were obtained with a Zeiss AxioImager.Z2 fluorescent microscope fitted with a 63x PlanApo objective and the Apotome.2 (Carl Zeiss Microscopy, Thornwood, NY). Images were prepared using Adobe Photoshop software.

Phylogenetics

All amino acid sequences for Arl13a were obtained from NCBI using the following access numbers: human (Hs; NP_001155963.1), mouse (Mm; NP_083223.1), rat (Rn; NP_001019537.1), chicken (Gg; XP_015134146.1), zebrafish (Dr; NP_957112.1), *Xenopus tropicalus* (Xt; XP_004916818.1), *Xenopus laevis* (Xl; AAH99310.1). Amino acid sequences of Arl13b from NCBI used the following accession numbers: human

(NP_001167621.1), mouse (NP_080853.3), rat (NP_001100571.1), chicken (XP_004938370.1), zebrafish (NP_775379.1), *Xenopus tropicalus* (NP_001184084.1). Accession numbers for Arl13 amino acid sequences were: worm (Ce; NP_001032986.1), and algae (Cr; XP_001691430.1). Sequence alignment was conducted using the online Multiple Sequence Comparison by Log-Expectation (MUSCLE) (McWilliam et al., 2013). Phylogenetic tree construction was performed using Phylodendron (http://iubio.bio.indiana.edu/treeapp/treeprint-form.html) with default parameters.

Imaging

In situ Images were obtained on a Zeiss AxioZoom.V16 fluorescence stereomacroscope using an AxioCam digital camera. Serial optical sections were obtained with a Zeiss AxioImager.Z2 fluorescent microscope fitted with a 63x PlanApo objective and the Apotome.2. Images were prepared using Adobe Photoshop.

RESULTS

To identify additional zebrafish homologs of *arl13b*, we searched the Ensembl Genome database (http://useast.ensembl.org/Danio_rerio/Info/Index) for paralogs and identified *arl13a* as a likely candidate. The *arl13a* gene is predicted to encode a 434 amino acid protein that is 28% identical to Arl13b. Both proteins are part of the Arl family of GTPases. Sequence alignment of Arl13a and Arl13b proteins from human, mouse, rat, chicken, frog, zebrafish, worm (Arl13) and *Chlamydomonas* (ARL13) found that sequence similarities were highest in the N-terminal region of the proteins, which contained the GTPase domain (Fig. 1). A highly conserved P loop (GLDNAGKT) required for nucleotide binding was located near amino acids 28–35 in most Arl13a and Arl13b homologs (Fig. 1, black bar). Phylogenetic comparisons revealed that Arl13a orthologs are more similar to each other and cluster separately from the Arl13b orthologs (Fig. 2). Furthermore, the *C. elegans* Arl13 gene and the *Chlamydomonas* Arl13 gene cluster with the tetrapod Arl13b genes, suggesting that Arl13b is more closely related functionally to the ancestral form.

The expression of *arl13a* and *arl13b* was examined by whole-mount *in situ* hybridization beginning at the 1-cell stage and progressing through 5 days post fertilization (dpf). Both *arl13a* and *arl13b* mRNAs were maternally expressed, although expression of *arl13b* was significantly higher (Fig. 3A, 1-cell). By the 1k-cell stage and through 50% epiboly, both genes were highly expressed throughout the blastula (Fig. 3A, 1k -cell, 50%). During somitogenesis, both *arl13a* and *arl13b* remained widely expressed throughout neural tissues. Beginning at 26 hours post fertilization (hpf), *arl13a* expression could be observed in the ventricular zone extending from a boundary in the midbrain, which was demarcated by *pax2a* expression (Fig. 3B, arrowhead), to the forebrain. We found that expression of *arl13a* was excluded from otic vesicles and the optic stalk, as no overlap was observed with *pax2a* expression (Fig. 3B, open arrow). A similar expression pattern was observed for *arl13b*, although faint expression was observed in the otic vesicle (Fig. 3F; open arrow). At 32–40 hpf, both *arl13a* and *arl13b* exhibited diffuse expression throughout the central nervous system (Figs. 3C and G). At 2 and 3 days post fertilization, the expression of *arl13a* remained diffusely expressed in neural tissues and appeared in the pronephros (Fig. 3D). At

4 dpf, expression of *arl13a* was no longer detected in the pronephros but was robust expression was observed in the olfactory pit and liver (Fig. 3E). By 5 dpf, expression had expanded into lower cranial structures. It is interesting to note that the expression of *arl13a* in the olfactory pit, liver, and cranial structures was considerably more robust than the neural expression at 2–3 dpf. The time required to detect *in situ* probe signal at 4–5 dpf was much shorter than the time needed to observe signal in neural tissues at earlier time points. Sense control probes did not result in detectable signal. In contrast, expression of *arl13b* remained elevated in neural tissues and the pronephros in 2 dpf, 3 dpf, and 5 dpf animals. In the retina, *arl13b* expression was observed through all cellular layers (Figs. 3H, I).

To determine the subcellular localization of Arl13a, mRNA encoding an Arl13a-mCherry fusion protein was injected into 1-cell zebrafish embryos. Embryos were fixed at the 6 somite stage and ciliated cells in presomitic mesoderm were analyzed by whole-mount immunocytochemistry. We first compared the subcellular localization of Arl13a to Arl13b by injected Arl13a-mCherry mRNA into the *Tg(−3.2actnb:arl13b-GFP)* transgenic line, which expresses an Arl13b-GFP fusion protein localizing to cilia (Borovina et al., 2010). The fluorescence signal from Arl13a-mCherry was observed in small puncta that showed considerable overlap with the signal from Arl13b-GFP, which is consistent with ciliary localization (Fig. 4A; arrow and arrowhead). To confirm that Arl13a localized to cilia, wild-type embryos were injected with Arl13a-mCherry mRNA and stained with acetylated tubulin. The Arl13a-mCherry fluorescence puncta partially overlapped with acetylated tubulin (Fig. 4B), indicating that Arl13a localized to cilia. Out of 150 cilia observed across 7 embryos, 79 cilia (53%) showed colocalization between Arl13a and acetylated tubulin and 71 (47%) were stained only with acetyled tubulin. To further define the spatial distribution of Arl13a, we used the *Tg(−3.2actnb:cetn4-GFP)* transgenic line that localizes to the basal bodies of cilia (Randlett et al., 2011; Ramsey and Perkins, 2013). The Arl13a-mCherry signal was immediately distal of signal from the centrin-GFP fusion protein in 3 of 4 cilia observed (Fig. 4C). The localization of Arl13a was also assessed in cells undergoing cell division in the presomitic mesoderm. Embryos were injected with Arl13a-mCherry mRNA and immunolabeled for α-tubulin to label microtubules of the mitotic spindle (Fig. 4D) or γ-tubulin to mark the centrosomes as the spindle poles (Fig. 4E). At each stage of the cell cycle, Arl13a-mCherry colocalized with α-tubulin to label microtubules of the mitotic spindle and the midbody (Fig. 4D). Arl13a was excluded from the spindle pole and did not colocalize with γ-tubulin.

We previously reported that *arl13b* mutants had mild retinal phenotypes during larval stages (Song et al., 2016). To determine if mutations in *arl13b* results in compensatory elevated expression of *arl13a,* we examined *arl13a* in *arl13b* mutants (Fig. 5). At both 48 hpf and 3 dpf, expression of *arl13a* was not significantly different between *arl13b* mutants and wild-type siblings (Figs 5A and 5B).

Discussion

Members of the Arf-like (Arl) subfamily of small GTPases are implicated in diseases known as ciliopathies (Zhang et al., 2013). While biochemical and functional studies have revealed important details about GTP-binding and the role of Arl2/3 and Arl13b proteins in protein trafficking, the Arl subfamily is large and questions about functional redundancy remain largely unanswered.

We previously reported that ciliary extension and long-term photoreceptor survival requires Arl13b (Song et al., 2016). Mutations in *ARL13B* cause Joubert Syndrome in humans (Cantagrel et al., 2008) and mice lacking *Arl13b* die in utero (Caspary et al., 2007). The Arl13b paralog, Arl13a, is a protein of unknown function and we questioned whether *arl13a* was expressed in similar domains as *arl13b* and could potentially provide functional compensation. While *arl13a* was expressed in a similar manner as *arl13b* during early zebrafish development, we did not observe expression in the retina or other neural tissues following somitogenesis. These results suggest that *arl13a* does not compensate for the loss of *arl13b* in the zebrafish retina. It is interesting to note, however, that Arl13a and Arl13b both localize to microtubules in ciliated and dividing cells of the developing zebrafish embryo. Arl13b directly binds tubulin and this interaction requires the N-terminal G-domain (Revenkova et al., 2018). As a small GTPase, Arl13a shares this G-domain and may also directly bind tubulin through this domain. As both genes exhibit overlapping expression patterns during early development, some functional redundancy may exist.

To date, this is the first study of Arl13a expression and cellular localization and no other functional studies have been conducted. The expression of *arl13a* in cranial structures is intriguing as craniofacial abnormalities are can be a symptom of Joubert Syndrome (Damerla et al., 2015). Loss of function studies will be required to identify the precise role of Arl13a and any functional redundancy in early development with Arl13b.

Acknowledgments

The authors would like to thank members of the Perkins lab for helpful discussions. This work was supported by the National Institutes of Health [NIH R01-EY017037 to B.D.P., NIH P30-EY025585 to Cole Eye Institute]; and the Research to Prevent Blindness [Doris and Jules Stein Professorship to B.D.P.].

References

Borovina A, Superina S, Voskas D, Ciruna B. 2010 Vangl2 directs the posterior tilting and asymmetric localization of motile primary cilia. Nat. Cell Biol 12:407–412. [PubMed: 20305649]

Cantagrel V, Silhavy JL, Bielas SL, Swistun D, Marsh SE, Bertrand JY, Audollent S, Attie-Bitach T, Holden KR, Dobyns WB, Traver D, Al-Gazali L, Ali BR, Lindner TH, Caspary T, Otto EA, Hildebrandt F, Glass IA, Logan CV, Johnson CA, Bennett C, Brancati F, Valente EM, Woods CG, Gleeson JG. 2008 Mutations in the cilia gene ARL13B lead to the classical form of Joubert syndrome. Am J Hum Genet 83:170–179. [PubMed: 18674751]

Caspary T, Larkins CE, Anderson KV. 2007 The graded response to Sonic Hedgehog depends on cilia architecture. Dev. Cell 12:767–778. [PubMed: 17488627]

Chiang AP, Nishimura D, Searby C, Elbedour K, Carmi R, Ferguson AL, Secrist J, Braun T, Casavant T, Stone EM, Sheffield VC. 2004 Comparative genomic analysis identifies an ADP-ribosylation factor-like gene as the cause of Bardet-Biedl syndrome (BBS3). Am J Hum Genet 75:475–484. [PubMed: 15258860]

Cuvillier A, Redon F, Antoine JC, Chardin P, DeVos T, Merlin G. 2000 LdARL-3A, a Leishmania promastigote-specific ADP-ribosylation factor-like protein, is essential for flagellum integrity. J Cell Sci 113 (Pt 11):2065–2074. [PubMed: 10806117]

Damerla RR, Cui C, Gabriel GC, Liu X, Craige B, Gibbs BC, Francis R, Li Y, Chatterjee B, San Agustin JT, Eguether T, Subramanian R, Witman GB, Michaud JL, Pazour GJ, Lo CW. 2015 Novel

Jbts17 mutant mouse model of Joubert syndrome with cilia transition zone defects and cerebellar and other ciliopathy related anomalies. Hum Mol Genet 24:3994–4005. [PubMed: 25877302]

Fan Y, Esmail MA, Ansley SJ, Blacque OE, Boroevich K, Ross AJ, Moore SJ, Badano JL, May-Simera H, Compton DS, Green JS, Lewis RA, van Haelst MM, Parfrey PS, Baillie DL, Beales PL, Katsanis N, Davidson WS, Leroux MR. 2004 Mutations in a member of the Ras superfamily of small GTP-binding proteins causes Bardet-Biedl syndrome. Nat Genet 36:989–993. [PubMed: 15314642]

Gotthardt K, Lokaj M, Koerner C, Falk N, Giessl A, Wittinghofer A. 2015 A G-protein activation cascade from Arl13B to Arl3 and implications for ciliary targeting of lipidated proteins. Elife 4.

Grayson C, Bartolini F, Chapple JP, Willison KR, Bhamidipati A, Lewis SA, Luthert PJ, Hardcastle AJ, Cowan NJ, Cheetham ME. 2002 Localization in the human retina of the X-linked retinitis pigmentosa protein RP2, its homologue cofactor C and the RP2 interacting protein Arl3. Hum Mol Genet 11:3065–3074. [PubMed: 12417528]

Hanke-Gogokhia C, Wu Z, Gerstner CD, Frederick JM, Zhang H, Baehr W. 2016a Arf-like Protein 3 (ARL3) Regulates Protein Trafficking and Ciliogenesis in Mouse Photoreceptors. J Biol Chem 291:7142–7155. [PubMed: 26814127]

Hanke-Gogokhia C, Zhang H, Frederick JM, Baehr W. 2016b The Function of Arf-like Proteins ARL2 and ARL3 in Photoreceptors. Adv Exp Med Biol 854:655–661. [PubMed: 26427472]

Hilgendorf KI, Johnson CT, Jackson PK. 2016 The primary cilium as a cellular receiver: organizing ciliary GPCR signaling. Curr Opin Cell Biol 39:84–92. [PubMed: 26926036]

Ishikawa H, Marshall WF. 2011 Ciliogenesis: building the cell's antenna. Nat Rev Mol Cell Biol 12:222–234. [PubMed: 21427764]

Jowett T 2001 Double in situ hybridization techniques in zebrafish. Methods 23:345–358. [PubMed: 11316436]

Li Y, Ling K, Hu J. 2012 The emerging role of Arf/Arl small GTPases in cilia and ciliopathies. J Cell Biochem 113:2201–2207. [PubMed: 22389062]

Li Y, Wei Q, Zhang Y, Ling K, Hu J. 2010 The small GTPases ARL-13 and ARL-3 coordinate intraflagellar transport and ciliogenesis. J Cell Biol 189:1039–1051. [PubMed: 20530210]

Liew GM, Ye F, Nager AR, Murphy JP, Lee JS, Aguiar M, Breslow DK, Gygi SP, Nachury MV. 2014 The intraflagellar transport protein IFT27 promotes BBSome exit from cilia through the GTPase ARL6/BBS3. Dev Cell 31:265–278. [PubMed: 25443296]

Lunt S, Haynes T, Perkins BD. 2009 Zebrafish ift57, ift88, and ift172 intraflagellar transport mutants disrupt cilia but do not affect Hedgehog signaling. Dev. Dyn in press.

Malicki JJ, Johnson CA. 2016 The Cilium: Cellular Antenna and Central Processing Unit. Trends Cell Biol

McWilliam H, Li W, Uludag M, Squizzato S, Park YM, Buso N, Cowley AP, Lopez R. 2013 Analysis Tool Web Services from the EMBL-EBI. Nucleic Acids Res 41:W597–600. [PubMed: 23671338]

Nachury MV, Loktev AV, Zhang Q, Westlake CJ, Peranen J, Merdes A, Slusarski DC, Scheller RH, Bazan JF, Sheffield VC, Jackson PK. 2007 A core complex of BBS proteins cooperates with the GTPase Rab8 to promote ciliary membrane biogenesis. Cell 129:1201–1213. [PubMed: 17574030]

Omori Y, Zhao C, Saras A, Mukhopadhyay S, Kim W, Furukawa T, Sengupta P, Veraksa A, Malicki J. 2008 Elipsa is an early determinant of ciliogenesis that links the IFT particle to membrane-associated small GTPase Rab8. Nat Cell Biol 10:437–444. [PubMed: 18364699]

Pathak N, Obara T, Mangos S, Liu Y, Drummond IA. 2007 The zebrafish fleer gene encodes an essential regulator of cilia tubulin polyglutamylation. Mol Biol Cell 18:4353–4364. [PubMed: 17761526]

Perkins BD, Nicholas CS, Baye LM, Link BA, Dowling JE. 2005 dazed gene is necessary for late cell type development and retinal cell maintenance in the zebrafish retina. Dev. Dyn 233:680–694. [PubMed: 15844196]

Ramsey M, Perkins BD. 2013 Basal bodies exhibit polarized positioning in zebrafish cone photoreceptors. J Comp Neurol 521:1803–1816. [PubMed: 23171982]

Randlett O, Poggi L, Zolessi FR, Harris WA. 2011 The oriented emergence of axons from retinal ganglion cells is directed by laminin contact in vivo. Neuron 70:266–280. [PubMed: 21521613]

Revenkova E, Liu Q, Gusella GL, Iomini C. 2018 The Joubert syndrome protein ARL13B binds tubulin to maintain uniform distribution of proteins along the ciliary membrane. J Cell Sci 131.

Roy S 2009 The motile cilium in development and disease: emerging new insights. Bioessays 31:694–699. [PubMed: 19492356]

Satir P, Christensen ST. 2007 Overview of structure and function of mammalian cilia. Annu. Rev. Physiol 69:377–400. [PubMed: 17009929]

Schrick JJ, Vogel P, Abuin A, Hampton B, Rice DS. 2006 ADP-ribosylation factor-like 3 is involved in kidney and photoreceptor development. Am J Pathol 168:1288–1298. [PubMed: 16565502]

Sharma N, Berbari NF, Yoder BK. 2008 Ciliary dysfunction in developmental abnormalities and diseases. Curr. Top. Dev. Biol 85:371–427. [PubMed: 19147012]

Song P, Dudinsky L, Fogerty J, Gaivin R, Perkins BD. 2016 Arl13b Interacts With Vangl2 to Regulate Cilia and Photoreceptor Outer Segment Length in Zebrafish. Invest Ophthalmol Vis Sci 57:4517–4526. [PubMed: 27571019]

Sun Z, Amsterdam A, Pazour GJ, Cole DG, Miller MS, Hopkins N. 2004 A genetic screen in zebrafish identifies cilia genes as a principal cause of cystic kidney. Development 131:4085–4093. [PubMed: 15269167]

Tsujikawa M, Malicki J. 2004 Intraflagellar transport genes are essential for differentiation and survival of vertebrate sensory neurons. Neuron 42:703–716. [PubMed: 15182712]

Veltel S, Gasper R, Eisenacher E, Wittinghofer A. 2008 The retinitis pigmentosa 2 gene product is a GTPase-activating protein for Arf-like 3. Nat Struct Mol Biol 15:373–380. [PubMed: 18376416]

Wiens CJ, Tong Y, Esmail MA, Oh E, Gerdes JM, Wang J, Tempel W, Rattner JB, Katsanis N, Park HW, Leroux MR. 2010 Bardet-Biedl syndrome-associated small GTPase ARL6 (BBS3) functions at or near the ciliary gate and modulates Wnt signaling. J Biol Chem 285:16218–16230. [PubMed: 20207729]

Wright ZC, Singh RK, Alpino R, Goldberg AF, Sokolov M, Ramamurthy V. 2016 ARL3 regulates trafficking of prenylated phototransduction proteins to the rod outer segment. Hum Mol Genet 25:2031–2044. [PubMed: 26936825]

Zhang Q, Hu J, Ling K. 2013 Molecular views of Arf-like small GTPases in cilia and ciliopathies. Exp Cell Res 319:2316–2322. [PubMed: 23548655]

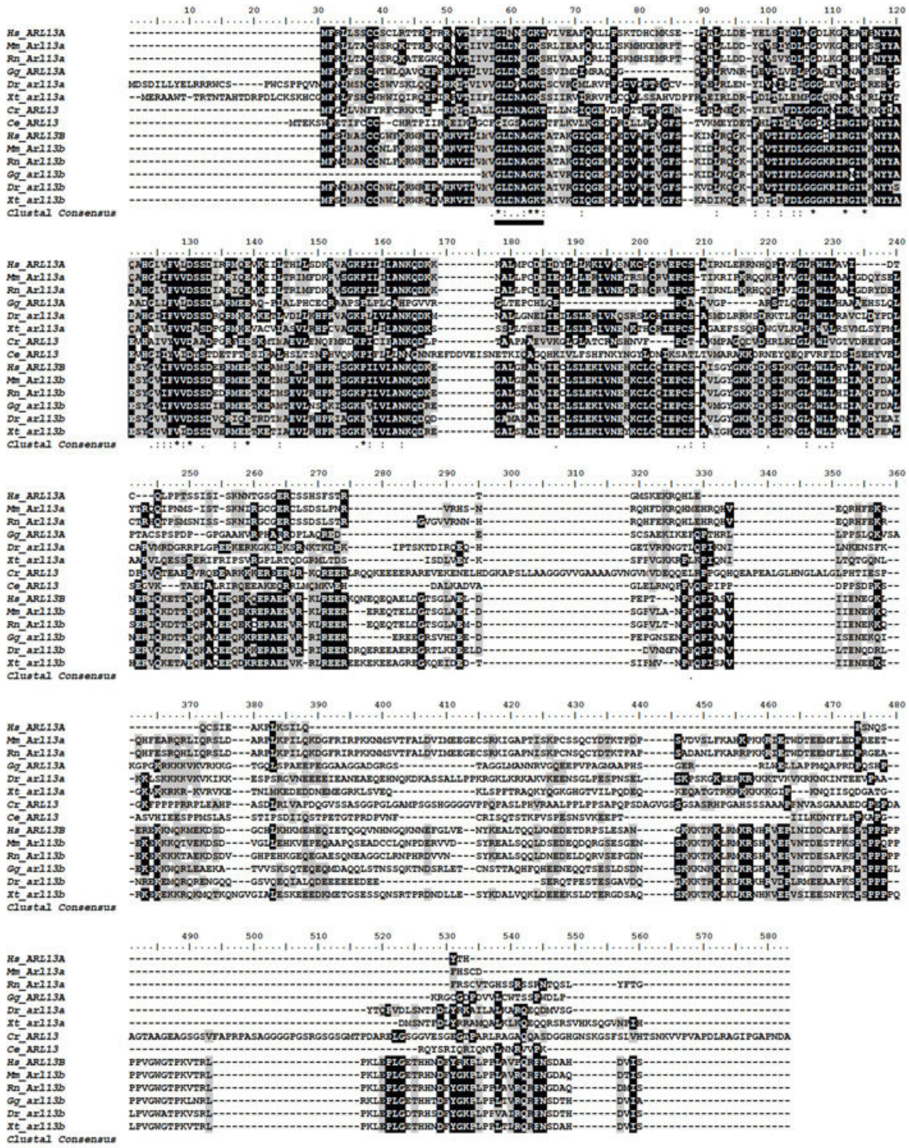

Figure 1. Sequence alignment of Arl13a and Arl13b shows strong similarity in the N-terminal region of the protein.

Using ClustalW, amino acid sequences for Arl13a homologs from human (Hs; NP_001155963.1), mouse (Mm; NP_083223.1), rat (Rn; NP_001019537.1), chicken (Gg; XP_015134146.1), zebrafish (Dr; NP_957112.1), *Xenopus tropicalus* (Xt; XP_004916818.1), *Xenopus laevis* (Xl; AAH99310.1), were aligned against amino acid sequences of Arl13b homologs from human (NP_001167621.1), mouse (NP 080853.3), rat (NP_001100571.1), chicken (XP_004938370.1), zebrafish (NP_775379.1), *Xenopus tropicalus* (NP_001184084.1), and Arl13 amino acid sequences from worm (Ce; NP 001032986.1), and algae (Cr; XP_001691430.1). Identical residues are noted in black and similar residues (minimum 50%) highlighted in gray. The nucleotide binding site (P loop) is underlined.

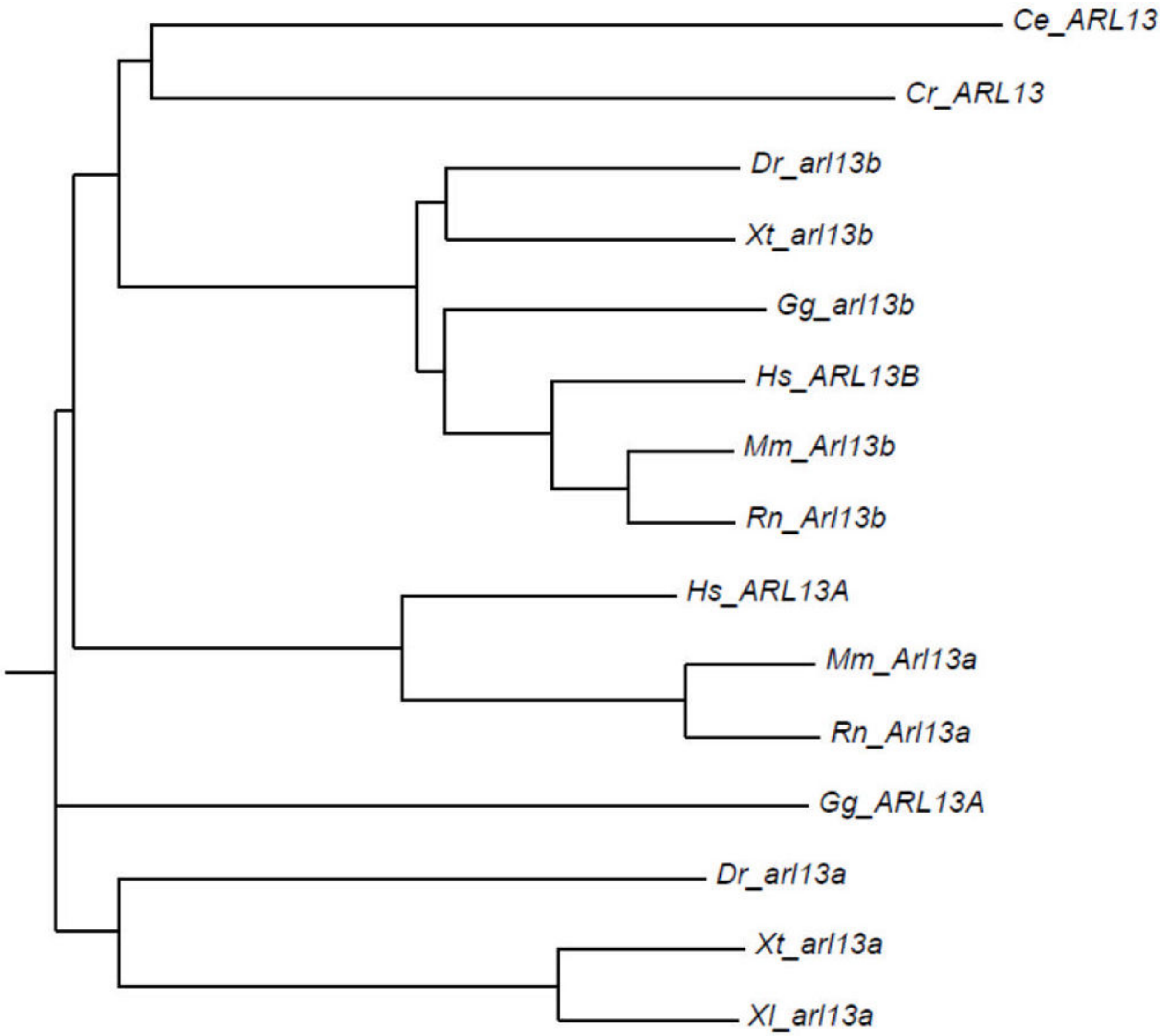

Figure 2. Phylogenetic relationship between Arl13 family members.

Phylogenetic tree was constructed using Phylodendron from an alignment of Arl13a and Arl13b amino acid sequences from *Chlamydomonas* (Cr), *C. elegans* (Ce), zebrafish (Dr), *Xenopus tropicalus* (Xt), chicken Gg), rat (Rn), mouse (Mm), and human (Hs).

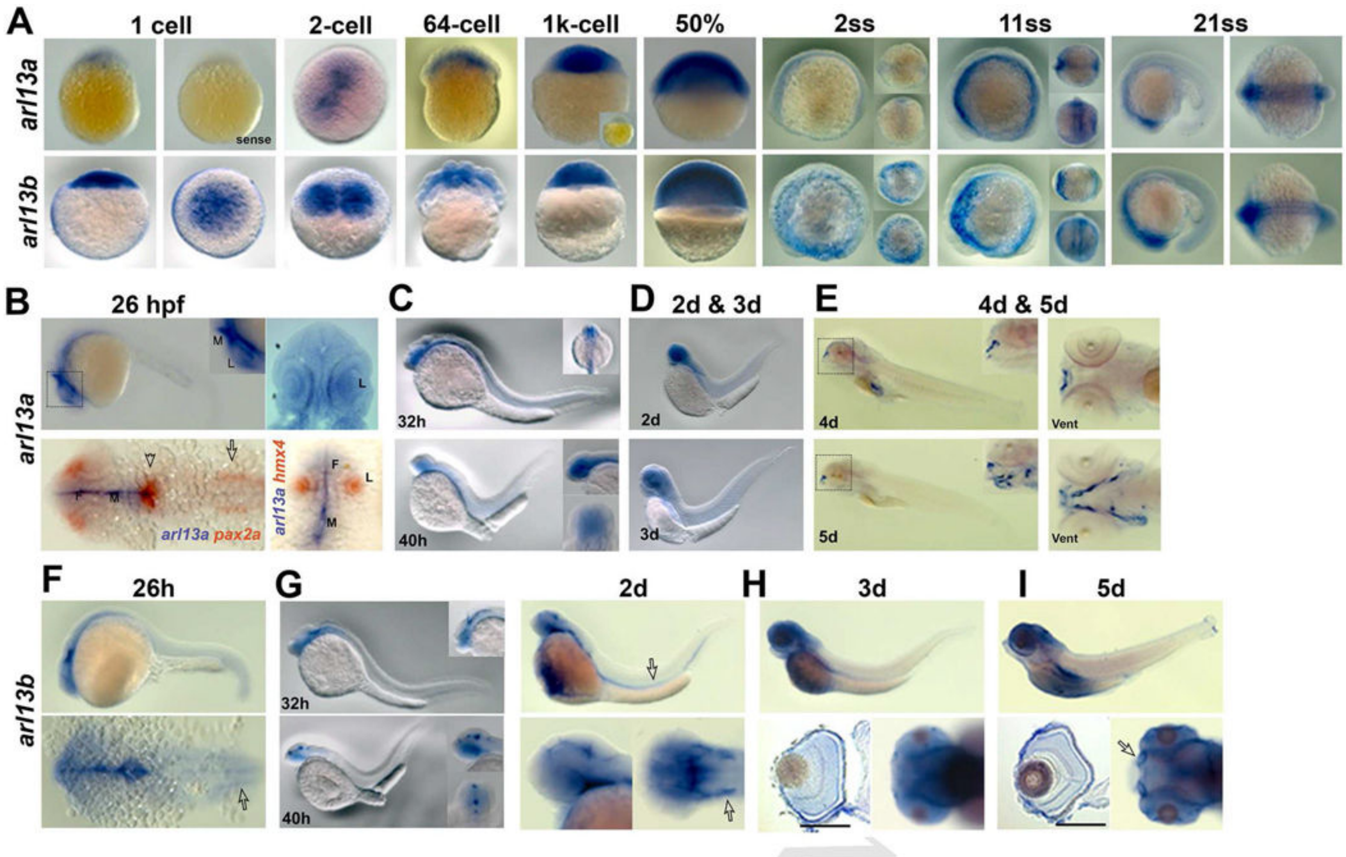

Figure 3. Developmental expression of zebrafish *arl13a* and *arl13b* from 1-cell to 5 dpf by *in situ* hybridization.

(A) Expression patterns of *arl13a* (top row) and *arl13b* (bottom row) from 1-cell stage to 21 somite stage (ss) using antisense RNA probes. Control (sense) RNA probes for *arl13a* are shown for 1-cell stage and for the 1k-cell stage embryos (inset). Anterior is to the left. For images of 2ss and 11ss embryos, dorsal views (upper inset) and front views (lower inset) are also shown. Views of 21ss specimens are lateral and dorsal views, respectively. (B) Expression of *arl13a* at 26 hpf. The upper panels show views of an embryo following whole-mount *in situ hybridization* noting expression the CNS. Upper left shows lateral view and upper right image is a dorsal view. Lower images show two-color *in situ* hybridization with *arl13a* (blue) and *pax2a* or *hmx4* (orange). Note that *arl13a* and *pax2a* expression domains do not overlap except in a small patch at the midbrain-hindbrain boundary (arrowhead). *arl13a* expression is excluded from the otic vesicle (open arrow) and in the lens, as noted by *hmx4* expression. (D) Expression of *arl13a* by WISH at 2 dpf (top) and 3 dpf (bottom). (E) *arl13a* is highly expressed at upper lip (insets from the black rectangle) and lower lip (right image, ventral view) at 4 dpf, and at jaw at 5dpf (lower images, inset is the higher magnification from the black rectangle). F, forebrain; M, midbrain; L, lens; Vent, ventral view. (F-I) Expression patterns of *arl13b* from 26 hpf to 5 dpf. In F, the arrow indicates the otic vesicles; G, the arrow (upper images) indicates kidney and the arrow (lower right) indicates otic vesicle; H and I, higher expression of *arl13b* at photoreceptor layer at 3 dpf and 5 dpf (sections, lower left images, respectively). I, arrow indicates olfactory bulbs at 5 dpf (lower right). Scale bar: 100 μm.

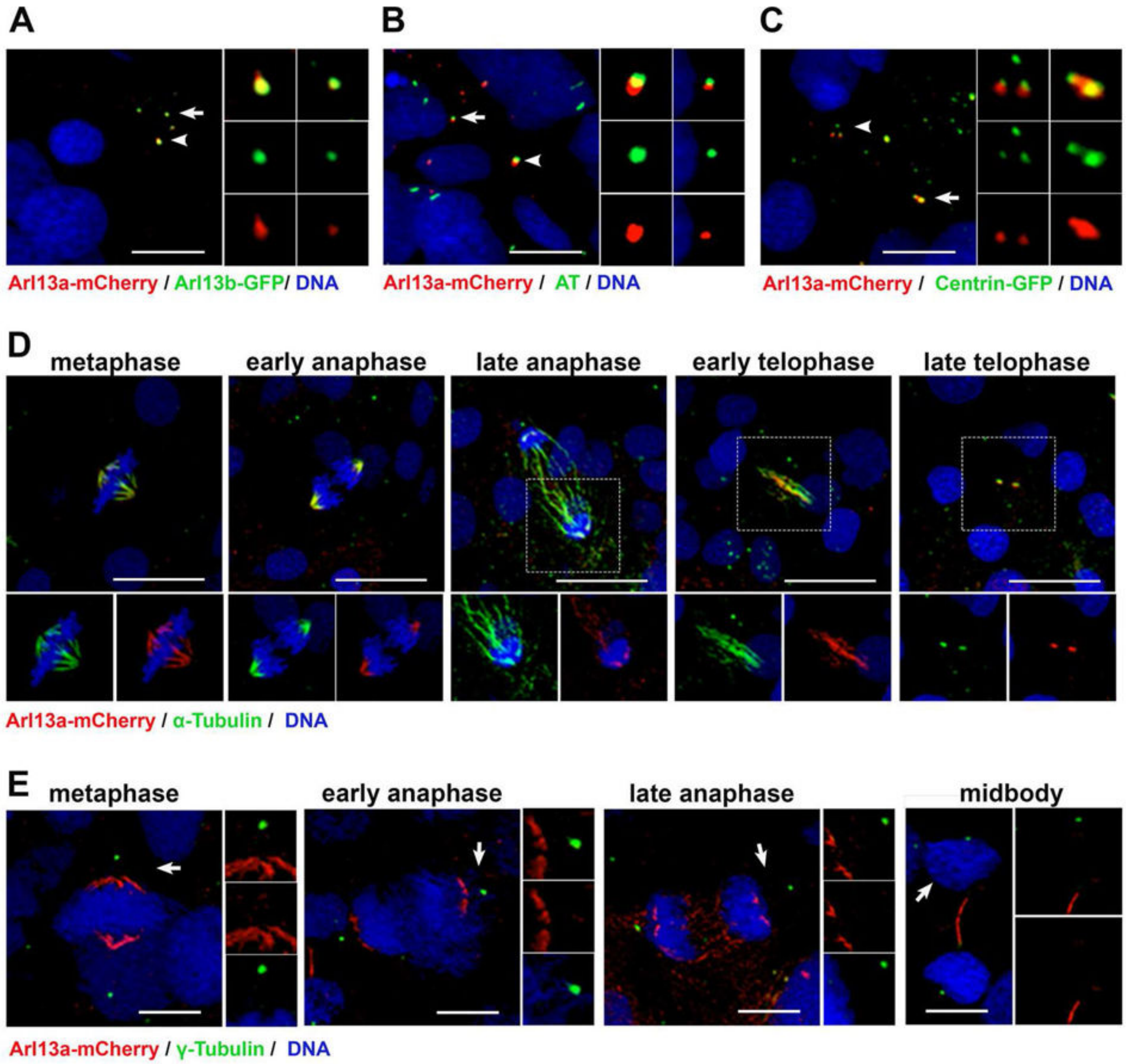

Figure 4. Arl13a colocalizes with microtubules in zebrafish embryos.

(A) *Tg(−3.2actnb:arl13b-GFP)* transgenic larvae injected with mRNA encoding Arl13a-mCherry were fixed at 6 somite stage (ss) and stained with antibodies against mCherry (red) or GFP (green). Cilia on two cells (arrow and arrowhead). Inset panels show enlarged images of individual channels and the merged image. (B) Wild-type larvae (6 ss) were fixed and stained with antibodies against mCherry (red) or acetylated-tubulin (green) to label cilia. (C) *Tg(−3.2actnb:cetn4-GFP)* transgenic larvae injected with mRNA encoding Arl13a-mCherry were fixed at 6 somite stage (ss) and stained with antibodies against mCherry (red) or GFP (green). (D)Mitotic cells in presomitic mesoderm of wild-type larvae (6 ss) were fixed and stained with antibodies against mCherry (red) or acetylated-tubulin (green) to label microtubules or (E) γ-tubulin to label centrosomes. All larvae were counterstained with DAPI to label nuclei. Scale bar: 10 µm (A-C); 20 µm (D, E).

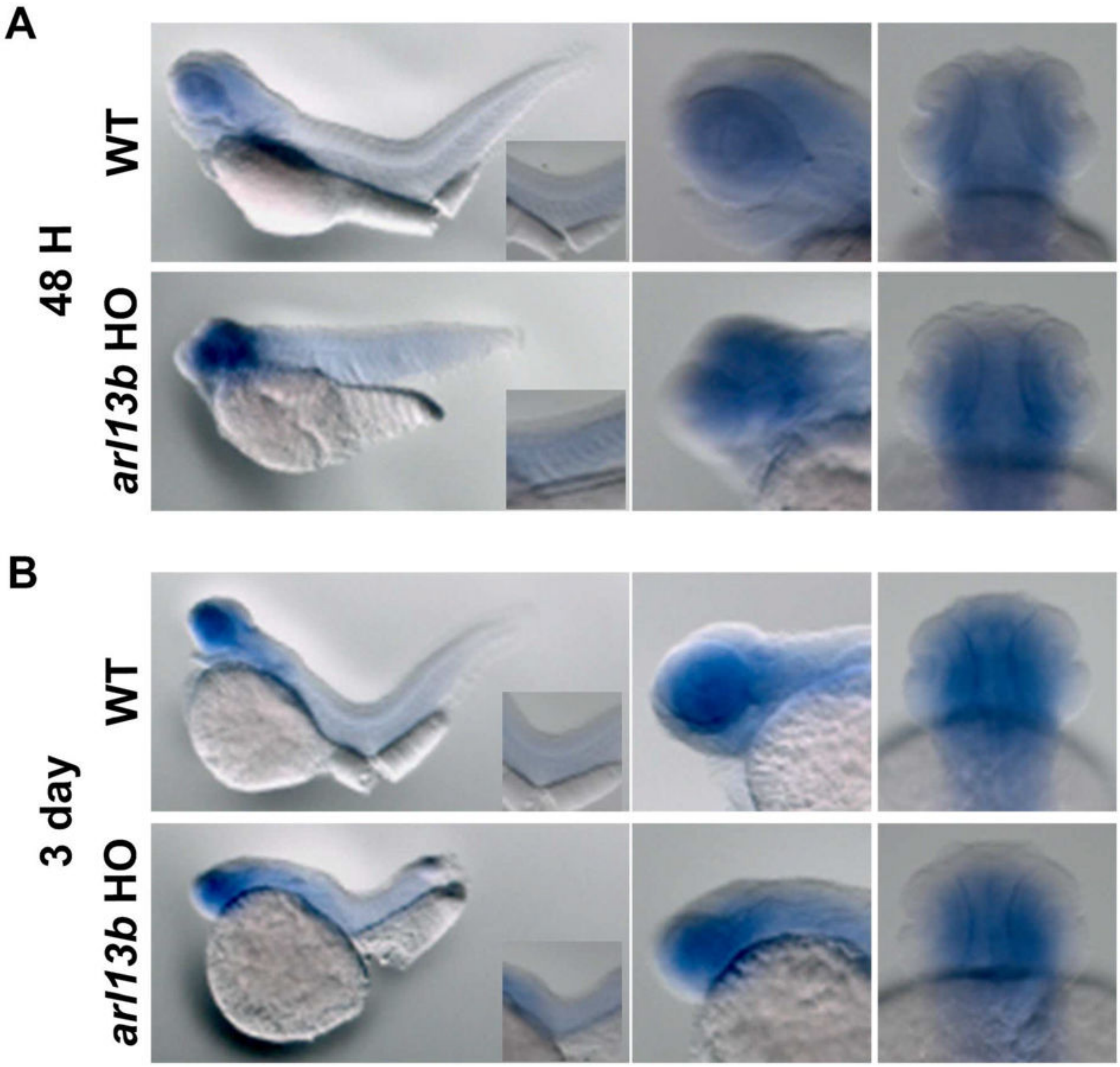

Figure 5. Expression of zebrafish *arl13a* in 48 hpf and 3dpf *arl13b*$^{-/-}$mutants by *in situ* hybridization.

(A) Expression of *arl13a* by WISH at 48 hpf and (B) 3 dpf in wild-type (top) and *arl13b* $^{-/-}$homozygous mutants (bottom). Lateral views are shown in left and middle panels. Right panels show the ventral views of the head. Insets of left panels show higher magnification of the trunk.